

# Cytoarchitecture and Myeloarchitecture of the sheep (*Ovis aries*) auditory cortex

Camille Pluchot<sup>1</sup>, Mélody Morisse<sup>1</sup>, Maryse Meurisse<sup>1</sup>, Jean-Marie Graïc<sup>2</sup>, Elodie

Chaillou<sup>1</sup>, Scott A. Love<sup>1</sup>

<sup>1</sup>INRAE, CNRS, Université de Tours, PRC, 37380, Nouzilly, France

<sup>2</sup>Department of Comparative Biomedicine and Food Science, University of

Padova, Legnaro

## **E-mail addresses, telephone number, ORCID, address of corresponding authors**

[pluchot.cam@gmail.com](mailto:pluchot.cam@gmail.com) ; 02.47.42.78.53; ORCID: <https://orcid.org/0009-0005-7532-6624>

[scott.love@inrae.fr](mailto:scott.love@inrae.fr) ; 02.47.42.75.00; ORCID: <https://orcid.org/0000-0001-7416-9210>

INRAE Centre Val de Loire

37380 Nouzilly

France

## **E-mail addresses and ORCID of co-authors**

[elodie.chaillou@inrae.fr](mailto:elodie.chaillou@inrae.fr) ; ORCID: <https://orcid.org/0000-0002-5577-8982>

[jeanmarie.graic@unipd.it](mailto:jeanmarie.graic@unipd.it) ; ORCID: <https://orcid.org/0000-0002-1974-8356>

[melody.morisse@inrae.fr](mailto:melody.morisse@inrae.fr)

[mary.meurisse1@free.fr](mailto:mary.meurisse1@free.fr)

**Short running title:** Sheep auditory cortex neuroanatomy

## **Acknowledgments**

We thank Frédéric Levy for helpful discussions in designing this research, Marie-Line Cateau for technical support, and Louise and Maurine Guilloteau, students from University Bachelor of Technology for their participation in the study. This work benefited from the equipment and expertise of the Imaging facility "Plateau d'Imagerie Cellulaire" (PIC) of UMR-PRC (<http://doi.org/10.17180/arap-gj59>). We acknowledge the financial support of the Agence Nationale de la Recherche (SheepVoicefMRI: ANR-20-CE20-0001-01) and the Institut National de Recherche pour l'Agriculture, l'Alimentation et l'Environnement Département Physiologie Animale et Systèmes d'Elevage.

## **Data Sharing and Data Availability**

The data generated during the current study are available in the associated Zenodo repository: 10.5281/zenodo.14824250. The repository includes compressed (quality 70%) versions of the scanned sections with their annotations (.czi file format) and spreadsheets containing layer thickness and cell diameter measurements. Compressed files are being made available, rather than uncompressed, to comply with the size limit of a Zenodo repository. The quality of the compressed images is more than sufficient to replicate the current results; however, uncompressed versions can be obtained from the authors.

## **Ethics approval statement**

This research was conducted in compliance with French and European guidelines for the housing and care of animals used for scientific purposes (European Union Directive 2010/63/EU). In accordance with the 3R principles of animal research, we chose to acquire the necessary biological tissue from animals that were reared and euthanized, independently of the present study; no experimental procedures were conducted on any live animals.

**Conflict of interest disclosure**

The authors have no relevant financial or non-financial interests to disclose.

## Abstract

The auditory cortex is central to auditory perception, but its detailed structural and functional organization in sheep (*Ovis aries*) has not been thoroughly investigated. In this study, we sought to address this gap by providing an in-depth overview of the cytoarchitecture and myeloarchitecture of the sheep auditory cortex, using cresyl violet staining and the neurochemical markers myelin basic protein and parvalbumin. Tissue samples from four sheep were used to characterize cortical layers, cellular composition, and myelination patterns, revealing a six-layered organization with variations in cell density and distribution. Myelin basic protein staining highlighted myelinated regions, providing insights into the myeloarchitecture, while parvalbumin staining identified the distribution of GABAergic interneurons, providing indications of the potential location of the primary auditory cortex. These findings deepen our knowledge of the auditory cortex in sheep, a key model for investigating sensory processing in large mammals. The structural and functional organization of the ovine auditory cortex aligns with findings in other mammals, suggesting that both are conserved across species and supporting the idea of evolutionary conservation in auditory processing mechanisms. However, future functional studies, using auditory stimulation paradigms, are necessary to fully understand the functional organization of this important sensory region.

### Keywords:

auditory cortex - ovine - parvalbumin - myelin basic protein - interneurons - posterior ectosylvian gyrus

## Introduction

In mammals, the auditory cortex is generally located bilaterally in the parieto-temporal regions of the brain. It is a hierarchically organized structure, consisting of several distinct subdivisions, each specialized in different aspects of auditory perception (Kaas, 2011). Central to these subdivisions, the primary auditory cortex is responsible for the initial cortical processing of auditory information.

Histological techniques, such as immunohistochemistry and neural tracing, have provided valuable insights into the cytoarchitecture and myeloarchitecture of the auditory cortex across various mammalian species (human: Hackett et al., 2001; non-human primate: Hackett et al., 2001; mouse: Anderson et al., 2009; cat: Winer & Prieto, 2001; rabbit: De Venecia et al., 1998; ferret: Bajo et al., 2007; gleaner bat: Martin del Campo et al., 2014; African wild dog: Chengetanai et al., 2020). These studies consistently show that the auditory cortex is organized into six distinct cortical layers, with variations in thickness, cellular composition and distribution (i.e., pyramidal neurons, interneurons, and glial cells, depending on the cortical layers).

Due to their social nature, sheep (*Ovis aries*) use sensory modalities such as hearing and vision for communication and environmental awareness, making them an interesting model for studying how the anatomy of mammalian brains is set up to process such sensory information. The sheep motor and somatosensory cortices have been extensively studied (Bagley, 1922; Dinopoulos et al., 1985; Gierthmuehlen et al., 2014; Johnson et al., 1974; King, 1911; Peruffo et al., 2019; Simpson & King, 1911; Woolsey & Fairman, 1946). The primary visual cortex of sheep has also received some attention (Clarke et al., 1976; Clarke & Whitteridge, 1976; Ebinger, 1975; Karamanlidis et al., 1979) and consists of a six-layered organization (Graïc et al., 2022), similar to that observed in other mammals (horses, monkeys, bottlenose dolphins: Graïc et al., 2022). However, the cytoarchitecture of the sheep auditory cortex remains largely unexplored.

To date, only two studies have investigated the location of the sheep auditory cortex. In the first study, Michaloudi and colleagues (1986) injected a horseradish peroxidase retrograde tracer into several areas of the posterior ectosylvian gyrus, in the parietal area of Rose (1942). When the tracer was injected into the anterior part of the posterior ectosylvian gyrus, labeled cells were found exclusively in the ventral division of the medial geniculate nucleus (MGNv), the final subcortical relay of auditory information before the auditory cortex. Based on this specific connection, they concluded that this injection site corresponded to the sheep auditory cortex. Decades later, Sahasrabuddhe and colleagues (2021) confirmed the auditory function of this region by recording cortical surface local field potentials in response to auditory stimuli. Together, these findings suggest that the sheep auditory cortex is located in brain areas homologous to those of other mammals (Kaas, 2011). Interestingly, the sheep has been used as a model for hearing loss using auditory brainstem responses in the fetal and perinatal phase (Cook et al., 1987; Griffiths et al., 1994; Pierson et al., 1994, 1995), or middle ear histology (Roberto et al., 1989), but no inquiry has been made further up the functional chain.

The present study aims to provide a detailed description of the cytoarchitecture and myeloarchitecture of the sheep auditory cortex, using the localization established by the two aforementioned studies (Michaloudi et al., 1986; Sahasrabuddhe et al., 2021). For this purpose, we employed cresyl violet ('Nissl') staining to define the number and thickness of cortical layers, as well as the composition and distribution of cells within each layer. Additionally, we assessed the distribution of Myelin Basic Protein (MBP), a marker of myelinated fibers, to investigate the cortical myeloarchitecture (Jeffrey et al., 1990). We also investigated the neurochemical properties of the sheep auditory cortex by quantifying the distribution of Parvalbumin (PV), a marker of GABAergic interneurons, which has been used to delineate the primary auditory cortex in various species (mice: Cruikshank et al., 2001; rabbits: McMullen et al., 1994; gerbils: Budinger et al., 2000; cats: Wallace et al., 1991; and monkeys: Jones et al., 1995, Kaas &

Hackett, 2000, Kosaki et al., 1997). Together, these approaches provide valuable insights into the structural and functional organization of the sheep auditory cortex.

## Materials and methods

### Tissue sampling

This research was conducted in compliance with French and European guidelines for the housing and care of animals used for scientific purposes (European Union Directive 2010/63/EU). In accordance with the 3R principles of animal research, we chose to acquire the necessary biological tissue from animals that were reared and euthanized, independently of the present study; no experimental procedures were conducted on any live animals. The brains of four Ile-de-France sheep (3 ewes: 13507, 13403, 13155; and 1 ram: 03133), between two and three years of age, were collected at a local slaughterhouse (UEPAO, <https://doi.org/10.15454/1.5573896321728955E12>; agreement number G37–175–2). The sheep were administered an intravenous injection of ketamine (5 mL). After confirming the loss of consciousness (i.e., absence of pupillary and palpebral reflexes), they were slaughtered by a licensed butcher. Then, the heads were immediately perfused in the carotid arteries with sodium nitrite at 37°C (2L per sheep, 1% in sodium chloride solution 0.9%), followed by 4% paraformaldehyde at 4°C (4L per sheep, in phosphate buffered saline (PBS), 0.1M, pH 7.4). The brain was extracted from the skull and post-fixed with 4% paraformaldehyde for 24h to 48h. It was washed in several PBS baths to remove excess paraformaldehyde, and immersed in a 20% sucrose cryoprotectant solution in PBS to prevent the formation of ice crystals during subsequent freezing. Each brain was cut in half sagittally, through the interhemispheric fissure. Then, each hemisphere was sectioned into a coronal orientation block of approximately two centimeters covering the auditory cortex area (i.e., posterior ectosylvian gyrus, Michaloudi et al., 1986). The boundaries of the auditory cortex were defined as follows: anteriorly by the sylvian

fissure and the anterior ectosylvian gyrus; posteriorly by the suprasylvian sulcus and the anterior part of the posterior sylvian gyrus; ventrally by the sylvian fissure; and dorsally by the suprasylvian sulcus (Figure 1). The blocks were frozen with dry ice (- 70°C) on the microtome stage, then cut into 40 µm thick coronal sections using a frozen microtome (Thermo Fisher Scientific, Sliding Microtome Microm HM 430, Germany). The coronal sections were stored at 4 degrees in PBS containing 0.1% sodium azide, until the respective staining protocols were performed.

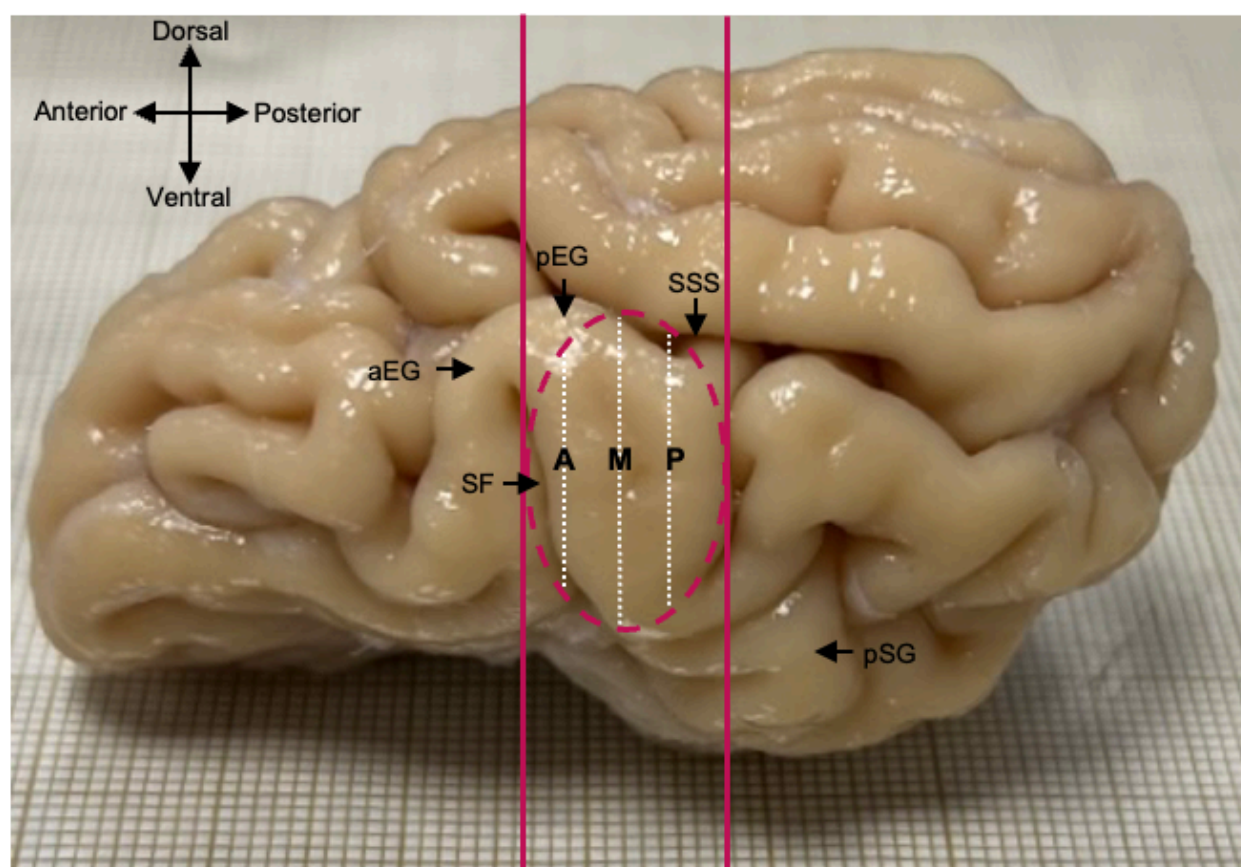


**Figure 1. Identification of the auditory cortex (dashed red circle) within the block delimited by the two vertical red lines.** *Lateral view of the left hemisphere of a sheep brain. Three sections of the auditory cortex (Anterior (A); Medial (M) ; Posterior (P)) per hemisphere, at comparable levels from one animal to another, were chosen for the analysis of each animal. Sylvian Fissure (SF), anterior Ectosylvian*



*Gyrus (aEG), posterior Ectosylvian Gyrus (pEG), Suprasylvian Sulcus (SSS) and posterior Sylvian Gyrus (pSG).*

### **Cresyl violet staining**

For each block, one out of twenty sections were mounted on gelatin glass slides and stained with cresyl violet (Nissl protocol) to visualize the cortical anatomy along the anterior-posterior axis of the sheep auditory cortex. First, sections were immersed in a 0.5% cresyl violet solution for 15 to 20 minutes and then rinsed twice with water to remove excess dye. The sections were then dehydrated in three successive baths of 95°C alcohol for two to seven minutes and three successive baths at 100°C alcohol for two to seven minutes. Finally, they were immersed in three successive baths of toluene for at least five minutes and coverslipped with Depex and scanned 48 hours later.

### **Immunohistochemistry**

Double labeling with parvalbumin (PV) and Myelin Basic Protein (MBP) was performed on the sections adjacent to those used for cresyl violet staining. Sections were permeabilized in PBS-Triton-Azide-BSA 1% (PBSTA-BSA) for one hour at room temperature. Then, they were incubated in the primary antibodies solution (monoclonal mouse anti-PV and monoclonal rat anti-MBP) for 48 hours at 37°C (Table 1). Then, sections were rinsed in four successive baths of PBS for ten minutes. They were incubated for three hours at 4°C with the secondary antibodies solution, containing donkey anti-mouse-CY3 and donkey anti-rat-488 (Table 1). Then, sections were rinsed in four successive baths of PBS for ten minutes. The sections were mounted on slides and oven-dried at 37°C for at least one day. They were coverslipped under Fluoromount-G® (Southern Biotechnology, Birmingham, AL), protected from light and scanned 48 hours later.

**Table 1. Primary and secondary antibodies used for the immunohistochemistry process**

	<b>Antibody</b>	<b>Immunogen</b>	<b>Manufacturing details</b>	<b>Dilution</b>
<b>Primary</b>	Mouse Anti-PV	Monoclonal mouse	Swant Cat# 235 RRID: AB_10000343	1:5000
	Rat anti-MBP	Monoclonal rat	Millipore Cat# MAB386 RRID: AB_94975	1:1000
<b>Secondary</b>	Donkey anti mouse-CY3	donkey	Jackson ImmunoResearch Labs Cat# 715-165-151 RRID: AB_2315777 minimal cross reaction with rat	1:1500
	Donkey anti rat-488	donkey	Jackson ImmunoResearch Labs Cat# 712-545-153 RRID: AB_2340684 minimal cross reaction with mouse	1:1500

### Microscopic imaging and section analysis

#### Cresyl violet staining: brightfield acquisition

Three sections per hemisphere, at comparable levels from one animal to another, were chosen for analysis: the first section was collected from the anterior (A), the second section from the medial (M), and the third from the posterior (P) part of the auditory cortex block (Figure 1). They were scanned using a digital slide scanner Axio Scan.Z1 (ZEISS®, Germany, with a 10x objective). Images acquired (.czi format) were analyzed with Zen® software (Zeiss, Germany). All images were aligned in the same orientation, with the cortical surface at the top and the white matter at the bottom. For each section, three regions of interest (ROIs) were defined: internal (IT), located in the dorsal part of the suprasylvian sulcus; intermediate (IM), located in the dorsal part of the external surface of the posterior ectosylvian gyrus and external (ET), located ventrally to the intermediate ROI on the posterior ectosylvian gyrus. These ROIs were drawn on relatively straight parts of the cortical surface using Zen® software (width: 1000 µm; height: 1250 to 2000 µm, depending on the distance between the cortical surface and white matter; Figure 2). Cortical layers within each ROI were identified based on cell density and

morphology. The thickness of each layer was measured and total cortical thickness for each ROI was obtained by summing the thicknesses of the six layers. All measurements are presented as mean  $\pm$  standard deviation, with the thickness of each layer also expressed as a mean percentage of the total cortical thickness. Data from the internal ROI of the posterior section of the right hemisphere of animal 03133 was missing from all analysis due to a cresyl violet staining issue. In addition, four layer thickness measurements that were either more than two times the interquartile range below the first quartile or above the third quartile were considered as outliers (*animal 13155: left, anterior section, intermediate ROI, Layer 1; animal 13507: left, medial section, internal ROI, Layer 4; animal 03133: right, posterior section, external ROI, Layer 6; animal 13403: right, medial section, internal ROI, Layer 1*). They were not included in layer thickness means and precluded the calculation of cortical thickness for the corresponding ROIs. For each animal, hemisphere, section, ROI, cortical layer and cell type, the diameters of five randomly selected cells were measured manually. The mean minimum and maximum diameters were then calculated across animals, hemispheres, sections, and ROIs for each layer and cell type. The percentage of the layer's surface covered by cresyl violet-stained cells was used to estimate cell density. Coverage of less than 25% was considered as low density, 25–75% moderate density, and more than 75% high density.

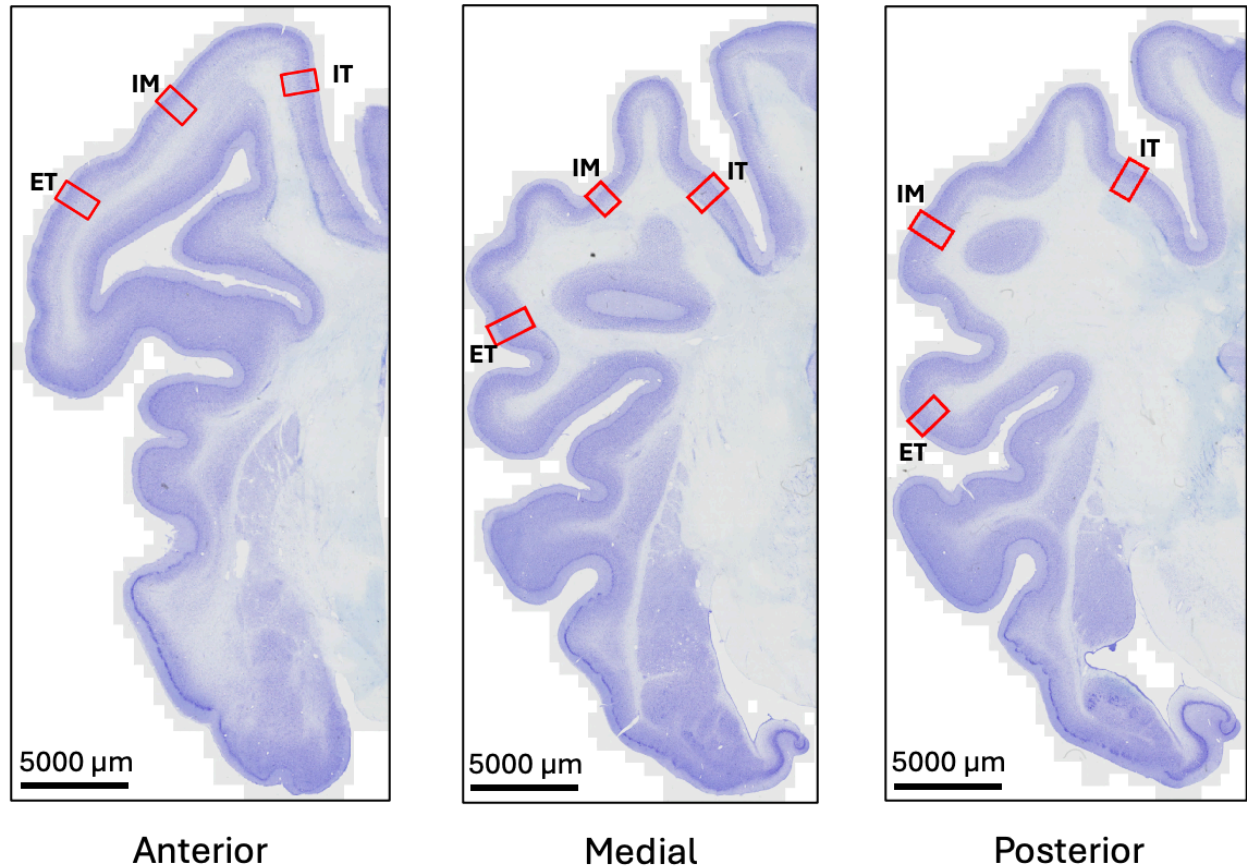


**Figure 2. Positioning of ROIs on the sheep auditory cortex sections.** *Internal (IT), intermediate (IM) and external (ET) ROIs were positioned on relatively straight parts of the cortical surface of the anterior, medial and posterior sections of the auditory cortex block. Images presented are from the left hemisphere of animal 03133.*

#### PV and MBP immunostaining: fluorescence acquisition

PV and MBP immunostaining were performed for both hemispheres of two animals (03133 and 13507), on slices adjacent to those selected as the three sections (anterior, medial, posterior) for cresyl violet staining. The immunostained sections were scanned using a digital slide scanner Axio Scan.Z1 (ZEISS®, Germany, with a 20x objective). The ROIs and cortical layers defined on cresyl violet stained sections were precisely reproduced on the immunostained sections using Zen® software. The acquired images (.czi format) were analyzed

with the open-source software QuPath (Bankhead et al., 2017). All images were aligned in the same orientation, with the cortical surface at the top and the white matter at the bottom. PV-immunoreactive (PV-ir) cell bodies within each ROI were automatically counted using QuPath (detection channel: CY3; Requested pixel size: 0.3256  $\mu\text{m}$ ; Nucleus parameter: 8  $\mu\text{m}$  background radius - 4  $\mu\text{m}$  median filter radius; Min area: 80  $\mu\text{m}^2$ ; Max area: 600  $\mu\text{m}^2$ ; Cell expansion: 2  $\mu\text{m}$ ; threshold: 950-15000). All measurements are presented as median cell density in each ROI. Similar to cresyl violet staining, densities of PV-ir cell bodies, PV-ir fibers and MBP-immunoreactive (MBP-ir) myelin were assessed based on the proportion of a layer's surface covered by the immunostaining (low: <25%, moderate: 25–75%, or high: >75%). Due to the high density of staining, precise measurement of PV-ir fiber length across layers was not possible. However, within each cortical layer it was possible to categorize fiber length as small (< 30  $\mu\text{m}$ ), medium (30 - 160  $\mu\text{m}$ ), or long (> 160  $\mu\text{m}$ ).

## Results

### Cresyl violet staining

Cresyl violet staining enabled the delineation of the cortical thickness (distance between the cortical surface and the white matter) of the ovine auditory cortex (Figure 2). No clear, consistent trends were observed that could account for the variability in total cortical thickness across animal, hemisphere, section or ROI (Figure 3). The mean total thickness of the auditory cortex was 1649  $\mu\text{m}$ , with a standard deviation of 205  $\mu\text{m}$ .

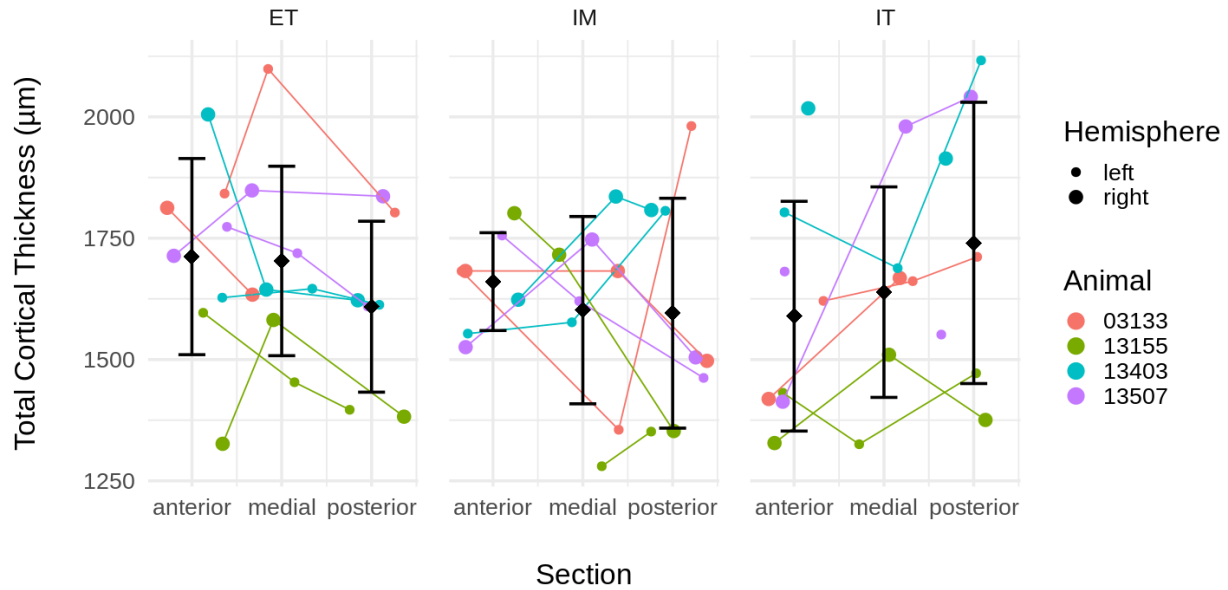


**Figure 3. Total cortical thickness (μm) of the sheep auditory cortex.** Total cortical thickness was measured within the three ROIs (ET, IM, IT) of the anterior, medial and posterior sections, for both hemispheres (indicated by point size), in four animals (distinguished by color). The total thickness of the auditory cortex varied between 1280 μm and 2116 μm across ROIs, sections, hemispheres, and animals.

### Layer identification

Examination of cellular organization revealed six cortical layers in the sheep auditory cortex. Each layer had distinct variations in cell density and morphology, which were consistent across sections and ROIs (Figure 4, Table 2). In detail, layer I was composed mainly of small, sparsely distributed glial cells, with mean diameters ranging from  $6.2 \mu\text{m} \pm 1.4$  to  $11 \mu\text{m} \pm 2.5$ . In addition, a few Cajal-Retzius cells were present, with diameters between  $12.1 \mu\text{m} \pm 2.2$  and  $18.7 \mu\text{m} \pm 2.9$  (Figure 4B). These cells were distributed throughout the layer. The boundary with layer II was easily distinguished by a clear change in cell type and density. Layer II was primarily characterized by granular cells, with diameters ranging from  $13.7 \mu\text{m} \pm 2.4$  to  $20.4 \mu\text{m} \pm 2.8$ . These cells were aggregated in strings throughout the layer. Additionally, a few pyramidal cells with triangular-shaped cell bodies were observed, with diameters ranging from  $13.8 \mu\text{m} \pm 2.3$  to

21.3  $\mu\text{m} \pm 3.3$  (Figure 4C). Both cell types were evenly distributed across the layer. Moving deeper into the cortex, the cell aggregation decreased, delineating the border between layers II and III. In layer III, spheroid granular cells (diameter: 14.4  $\mu\text{m} \pm 2.2$  - 19.7  $\mu\text{m} \pm 2.5$ ) were more numerous than pyramidal cells (diameter: 14.6  $\mu\text{m} \pm 2.2$  - 21.8  $\mu\text{m} \pm 3$ ), both were distributed throughout the layer (Figure 4D). Distinguishing between layers III and IV proved challenging. However, a slight decrease in overall cell density could be observed in layer IV compared to layer III. In layer IV, spheroid granular cells (mean diameter: 14.9  $\mu\text{m} \pm 2.2$  - 21.5  $\mu\text{m} \pm 3.1$ ) were more numerous than pyramidal cells (mean diameter: 13.3  $\mu\text{m} \pm 2$  - 19.6  $\mu\text{m} \pm 3$ ), both distributed throughout the layer (Figure 4E). The upper part of layer V contained a few large pyramidal cells (Figure 4F, mean diameter: 23.2  $\mu\text{m} \pm 3.8$  - 33.4  $\mu\text{m} \pm 5.2$ ), which marked the distinction between layers IV and V. Layer V also consisted of smaller pyramidal cells (mean diameter: 14.1  $\mu\text{m} \pm 2.2$  - 19.6  $\mu\text{m} \pm 3$ ) and a larger number of spheroid granular cells (mean diameter: 14.5  $\mu\text{m} \pm 2$  to 20.8  $\mu\text{m} \pm 2.9$ ), both distributed throughout the layer (Figure 4F). A slight increase in overall cell density could be observed in layer VI compared to layer V. Layer VI contained both spheroid granular cells, with mean diameters ranging from 14.5  $\mu\text{m} \pm 2.3$  to 19.8  $\mu\text{m} \pm 2.7$ , and pyramidal cells, with mean diameters from 13.9  $\mu\text{m} \pm 2.2$  to 20.7  $\mu\text{m} \pm 3.3$ , both distributed throughout the layer (Figure 4G). Additionally, this layer included spindle-shaped granular cells arranged parallel to the interface with the white matter, aligned along their long axis (Figure 4G').

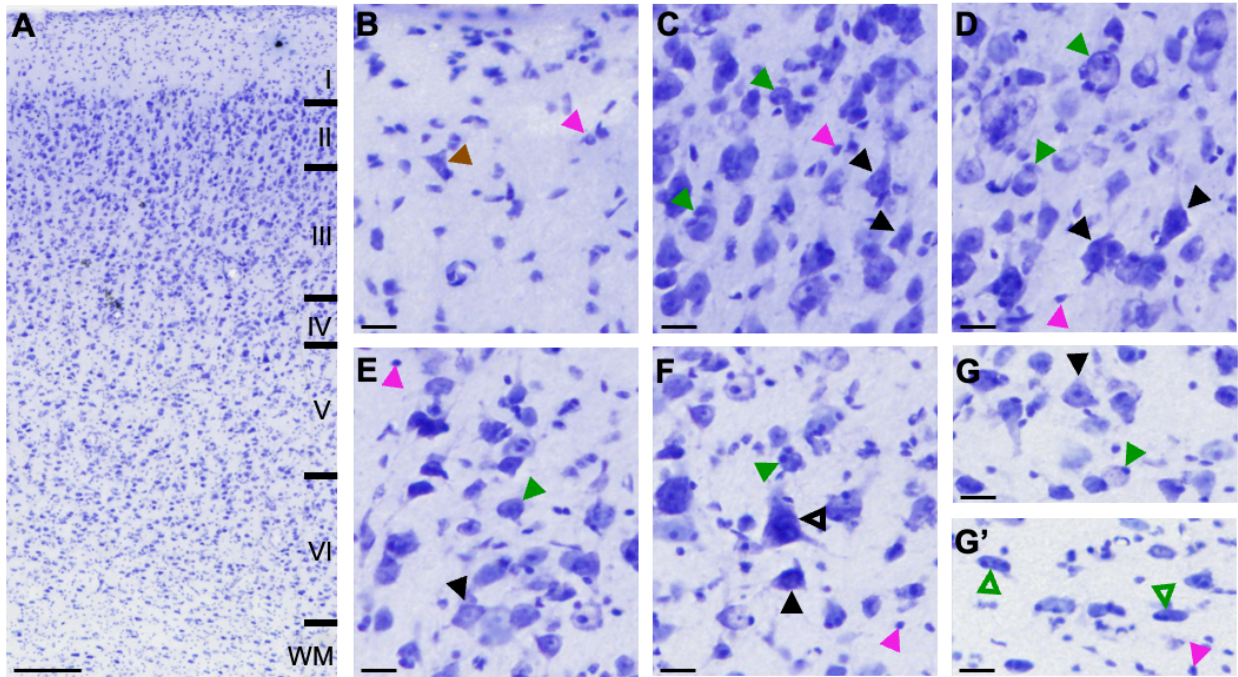


**Figure 4. Nissl-stained section of the sheep auditory cortex.** A- Identification of six cortical layers (I, II, III, IV, V, VI) and the white matter (WM); B- Glial cells (pink arrowhead) and Cajal-Retzius cells (brown arrowhead) of layer I; Spheroid granular cells (green arrowhead) and pyramidal cells (black arrowhead) of layers II (C), III (D), IV (E), V (F) and VI (G); Large pyramidal cells of layer V (unfilled black arrowhead); G'- Spindle-shaped granular cells of layer VI (unfilled green arrowhead). Note that glial cells were present in all six layers (pink arrowheads). Data shown is from the external ROI, of the anterior section, of the left hemisphere, of animal 03133. Scale bars: 200  $\mu$ m (A); 20  $\mu$ m (B-G').

Based on this cellular organization, the thickness of each of the six cortical layers across sections, for each ROI and hemisphere of the four animals was measured (Figure 5). Layers II and IV were the thinnest ( $131 \mu\text{m} \pm 30$ ;  $181 \mu\text{m} \pm 45$ , respectively) and exhibited the lowest variability. These two layers represented 7.9 and 10.9 % of the total thickness, respectively. Layer I was thicker ( $282 \mu\text{m} \pm 71$ ) and showed slightly more variability than layers II and IV. The mean thicknesses of layers III and V were similar ( $342 \mu\text{m} \pm 79$ ;  $341 \mu\text{m} \pm 88$ , respectively) while layer VI was the thickest ( $376 \mu\text{m} \pm 136$ ) of all layers. The variability observed in the



thicknesses of layers I, III, V, and VI did not appear to be linked to any specific criterion, such as ROIs, sections, hemispheres, or animals. Overall, the mean percentage of total cortical thickness of layers I, III, V and VI was similar, ranging from 17.1 to 22.8 % (Table 2).

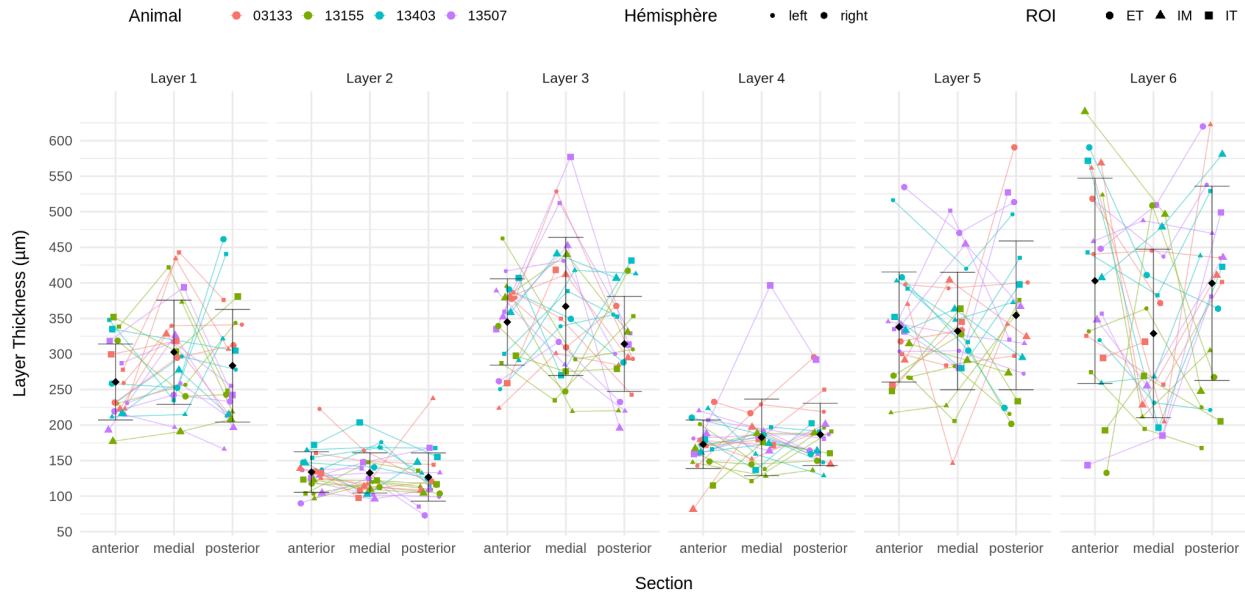


**Figure 5. Thickness (µm) of the six cortical layers in the sheep auditory cortex.** Thickness of each cortical layer was measured for the anterior, medial and posterior sections within the three ROIs (IT - IM - ET, indicated by different shapes). Measurements were performed for both hemispheres (indicated by point size), in four animals (distinguished by color). No clear, consistent trends in layer thickness were observed across either animal, hemisphere, section or ROI.

**Table 2. Cortical organization of the sheep auditory cortex**

Layer	Cresyl violet						Myelin Basic Protein		Parvalbumin					
	Mean thickness		Cell		Mean cell diameter (µm)		Fiber		Cell		Mean cell diameter (µm)		Fiber	
	µm	%	Type	Density	Min	Max	Density	Orientation relative to the cortical surface	Density	Type	Min	Max	Density	Orientation relative to the cortical surface
I	282 ±71	17.1 ±4.3	Glial	Moderate	6.2±1.4	11±2.5	Low	Parallel	Ø	Ø	Ø	Ø	Low	Perpendicular
			Cajal	Low	12.1±2.2	18.8±3								Parallel
II	131 ±30	7.9 ±1.8	Granular	High	13.6±2.6	20.4±3.5	Low	Perpendicular	Low	Spheroid	15.4±3	19.2±3.7	Moderate	Perpendicular
			Pyramidal	Low	13.7±2.6	21.3±3.3				Polygonal	18±5.6	22±4.5		Parallel
III	342 ±9	20.7 ±4.8	Granular	Moderate	14.9±2.2	21.5±3.1	Moderate / High	Perpendicular	High	Spindle-shaped	22.3±2	22.8±2.4	High	Parallel
			Pyramidal	Moderate	14.6±2.2	21.8±3				Spheroid	14.8±1.8	18.9±2		Perpendicular
IV	181 ±45	10.9 ±2.7	Granular	Moderate	14.4±2.2	19.7±2.5	Moderate / High	Perpendicular	Moderate	Polygonal	18±2.2	24.5±3.6	High	Parallel
			Pyramidal	Moderate	13.3±2	19.6±3				Spindle-shaped	21.9±3.3	24±2.8		Perpendicular
V	341 ±88	20.6 ±5.3	Granular	Moderate	14.5±2	20.8±2.9	High	Perpendicular	High	Spheroid	14.5±2.5	17.4±2.6	High	Parallel
			Pyramidal	Moderate	14.1±2.2	19.6±3				Polygonal	17.8±2.7	25±4.1		Perpendicular
VI	376 ±136	22.8 ±8.2	Large Pyramidal	Low	23.2±3.8	33.4±5.2	Moderate	Perpendicular	Moderate	Spindle-shaped	20.4±2.9	23.1±4.1	Moderate	Parallel
			Granular	Moderate	14.5±2.3	19.8±2.7				Spheroid	15±1.9	19.2±3		Perpendicular
VII	376 ±136	22.8 ±8.2	Pyramidal	Moderate	13.9±2.2	20.7±3.3	Moderate	Perpendicular	Moderate	Polygonal	20.2±3.1	27.7±3.8	Moderate	Parallel
			Granular	Moderate	14.5±2.3	19.8±2.7				Spindle-shaped	20.5±3.2	24.1±3.7		Perpendicular

## MBP immunostaining

In the sheep auditory cortex, MBP-ir myelin was observed for all animals, hemispheres, sections and ROIs. MBP-ir myelin was present in all six cortical layers (Figure 6). MBP immunostaining revealed fibers oriented parallel to the cortical surface in the upper part of layer I (Figure 6B'), whereas fibers oriented perpendicular to the cortical surface were observed traversing layers II to VI (Figure 6B).

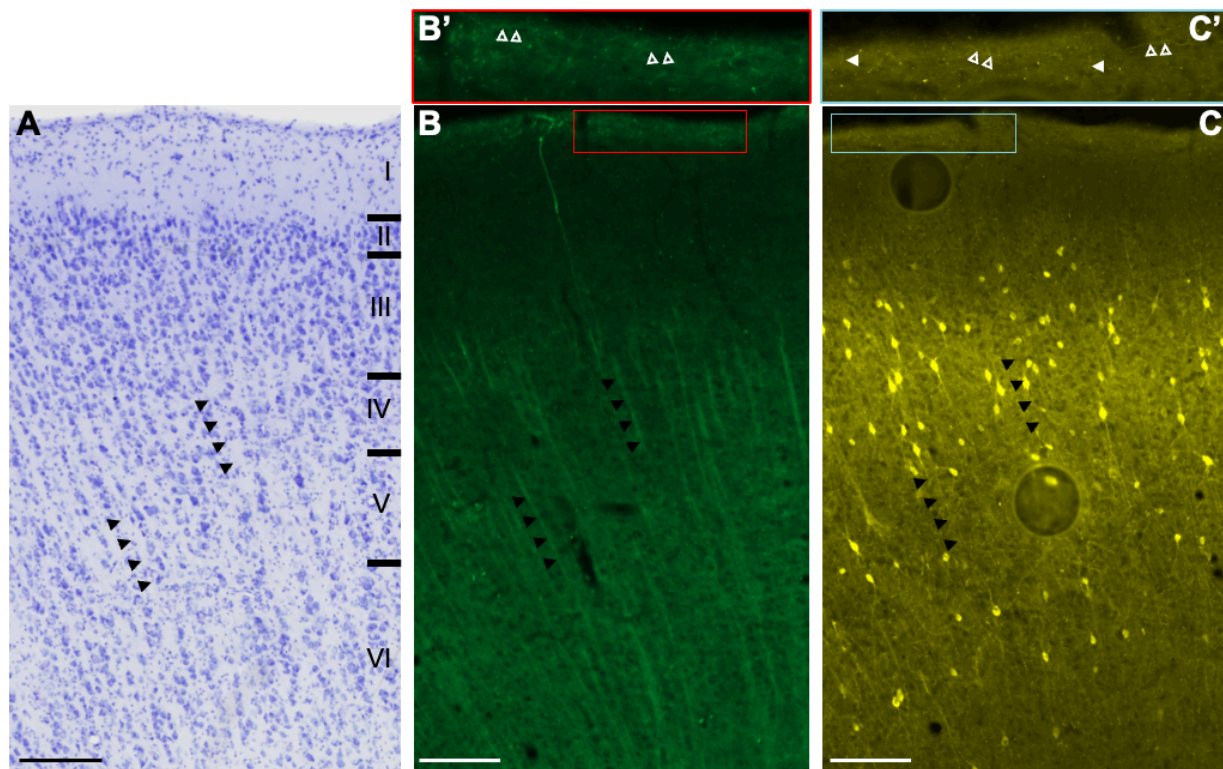


**Figure 6. Orientation of fibers and cells in the sheep auditory cortex.** A- Cresyl violet staining revealed cells aligned perpendicular to the cortical surface; B- MBP staining highlighted fibers with a similar perpendicular orientation (black arrowheads) and B' parallel fibers in the upper part of layer I (unfilled white arrowhead); C- PV staining revealed fewer perpendicular fibers and cell bodies, and C'- fibers parallel to the cortical surface (unfilled white arrowhead) in the upper part of layer I. Data shown is from the external ROI, of the posterior section, of the left hemisphere, of animal 13507. Black arrowheads in A-, B- & C- indicate equivalent locations and were defined based on the fibers in B-. Scale bars: 200  $\mu$ m (A, B & C); 50  $\mu$ m (B' & C').

No clear differences in MBP immunostaining across hemispheres, sections, and ROIs were observed for layers I, II, V, and VI. Layers I and II consistently contained a low density of MBP-ir myelin, while layer VI exhibited a moderate density, and layer V a high density. In contrast, layers III and IV showed greater variability in their MBP-ir density. Layer III contained either a moderate or high density of MBP-ir but with a notable prevalence of high density (Figure 7A). Layer IV contained moderate or high MBP-ir myelin density, with moderate density mainly in external ROIs (Figure 7B), high density predominantly in internal ROIs, while intermediate ROIs had an equal distribution of moderate or high MBP-ir myelin density.

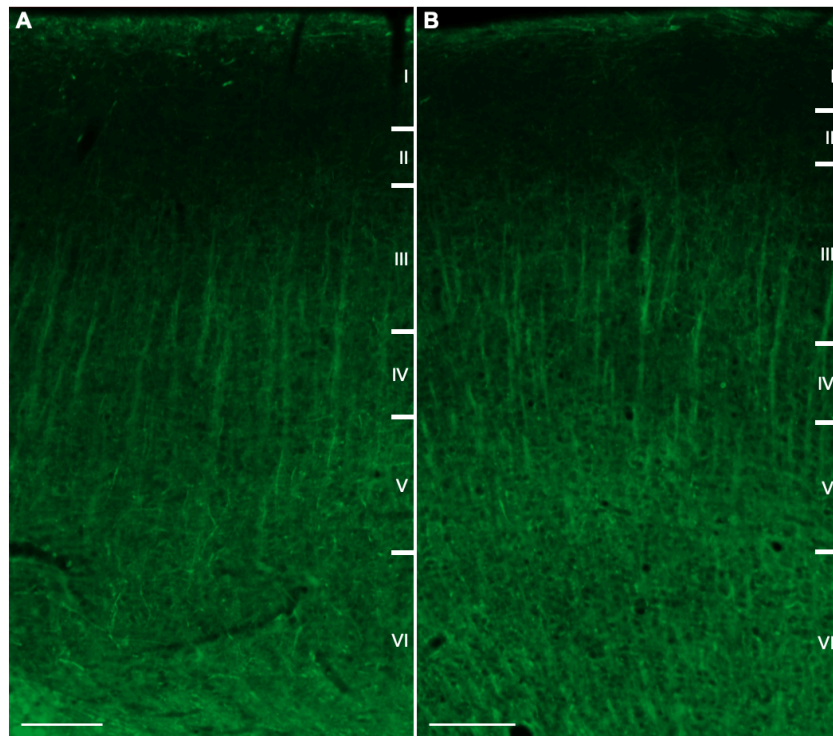


**Figure 7. MBP-ir myelin distribution in the internal (A) and external (B) ROIs of the anterior section of the sheep auditory cortex.** A- Internal ROI: low density of MBP-ir myelin in layers I and II, moderate density in layer VI, and high density in layers III-V; B- External ROI: low density of MBP-ir myelin in layers I - II, moderate density in layers IV and VI, and high density in layers III and V. Cortical layers, defined using cresyl violet-stained sections, were precisely reproduced onto the immunostained sections. Data shown is from the left hemisphere of animal 13507. Scale bars: 200  $\mu$ m (A & B).

## PV immunostaining

PV-ir immunostaining revealed fibers and cell bodies distributed throughout the sheep auditory cortex. In general, a dorsoventral gradient of staining was observed, with the highest density being observed in the dorsal part of the posterior ectosylvian gyrus between the internal and intermediate ROIs (Figure 8, Supplementary Figure 1). The dorsoventral gradient decreased abruptly into the suprasylvian sulcus, with a nearly complete absence of cell body staining after the internal ROI. On the outer cortical surface of the posterior ectosylvian gyrus, the gradient decreased more gradually, with the external ROI exhibiting an almost complete absence of cell body staining (Figure 8D). However, short PV-ir fibers were still observed in this ROI despite the lack of stained cell bodies.

In the majority of the internal and intermediate ROIs, medium to long fibers were observed in layers I and II, whereas layers III, IV, V and VI contained predominantly long fibers (Figure 8E). The highest density of PV-ir fibers was observed in layers III, IV and V, followed by layers II and VI, and the lowest in layer I. Across all six cortical layers, fibers oriented both perpendicular and parallel to the cortical surface were observed, with more perpendicular (Figure 8E). Fibers with diverse orientations were also observed in the upper part of layer I (Figure 6C'). In addition, large basket-like structures were observed around unstained cell bodies in the upper part of layer V, with a mean diameter ranging from  $34.8 \mu\text{m} \pm 8.7$  to  $42.9 \mu\text{m} \pm 8.3$  (Figure 8H).

PV-ir cell bodies were observed in layers II, III, IV, V, and VI, but not in layer I (Figure 8B-C). They were GABAergic interneuron cell bodies, including spheroid, polygonal, and spindle-shaped (Table 2, Figure 8F-I). The density of PV-ir cell bodies varied across sections and ROIs. The highest median density was found in the intermediate ROI ( $65.9 \text{ cells/mm}^2$ ), followed by the internal ROI ( $50.2 \text{ cells/mm}^2$ ), and the lowest density in the external ROI ( $17.2 \text{ cells/mm}^2$ , Figure 8B-D).

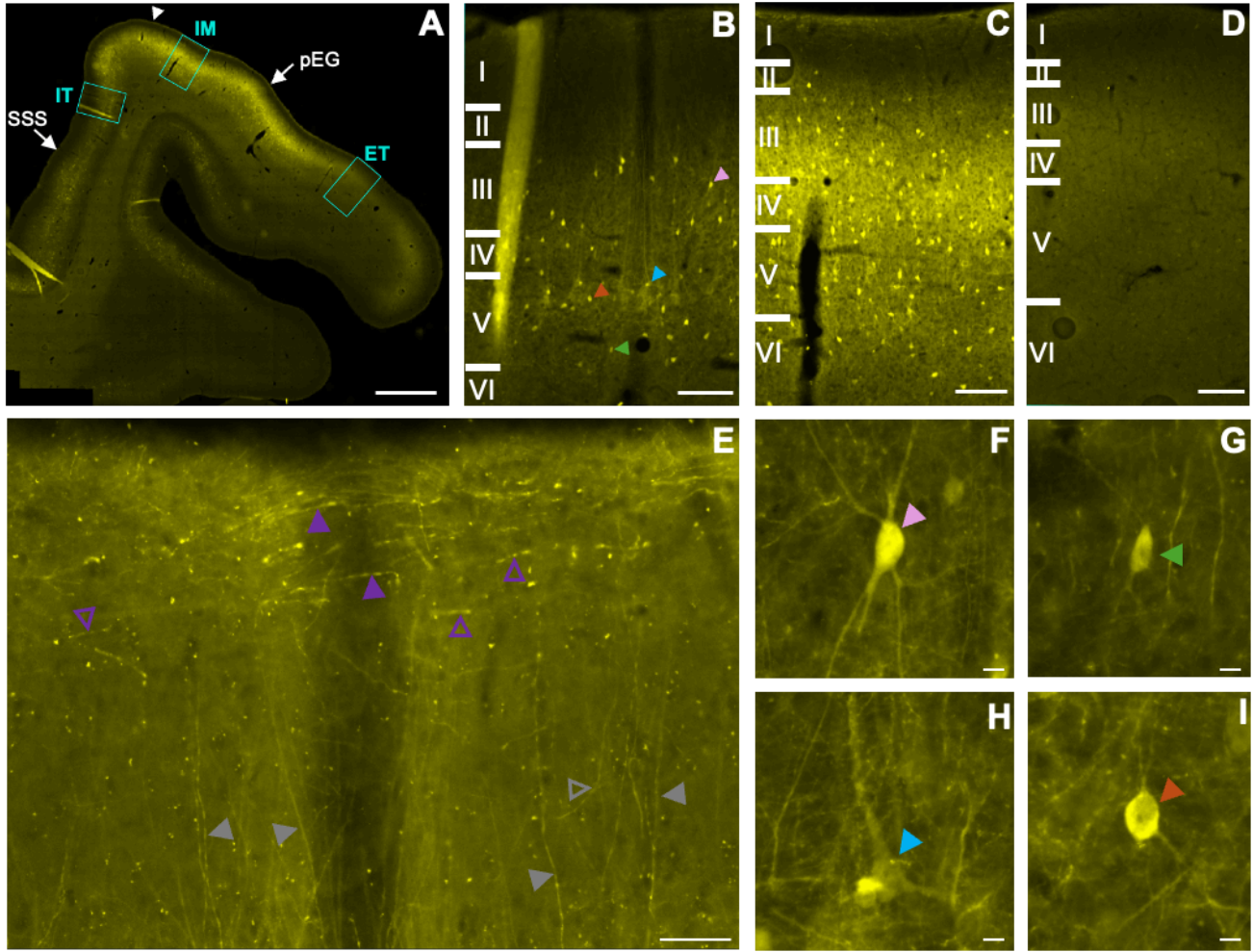


**Figure 8. Distribution of PV-ir cell bodies and PV-ir myelin in the sheep auditory cortex.** A- The dorsoventral gradient of PV staining in the anterior section of the right hemisphere of animal 13507, with the three ROIs (IT: internal, IM: intermediate, ET: external) indicated in blue. The highest density of PV staining was observed in the dorsal part of the posterior ectosylvian gyrus (white arrowhead). The gradient decreased abruptly into the suprasylvian sulcus (SSS) and more gradually along the outer cortical surface (pEG). B-D- Distribution of PV staining in the three ROIs. E- PV-ir fiber orientation and length, revealing long (filled grey arrowhead) and medium (unfilled grey arrowhead) perpendicular fibers, medium (filled purple arrowhead) and short (unfilled purple arrowhead) parallel fibers. F-I: GABAergic PV-ir cell bodies; F- polygonal interneuron with axonal projections (pink arrowhead); G- spindle-shaped interneuron (green arrowhead); H) basket-like structure (blue arrowhead) and I- spheroid interneuron (orange arrowhead). NOTE: The highest density of PV was observed in the IM ROI, followed by the IT ROI, and no PV-ir cell-bodies in the ET ROI. Scale bars: 2000  $\mu$ m (A); 200  $\mu$ m (B-D); 50  $\mu$ m (E); 10  $\mu$ m (F-I).



The density of PV-ir cell bodies varied by layer, with the highest density in layers III and V, followed by a moderate density in layers IV and VI, a low density in layer II, and no interneurons in layer I (Figure 8C). In detail, layer II consisted of a sparse distribution of spheroid interneurons (mean diameter:  $15.4 \mu\text{m} \pm 3$  -  $19.2 \mu\text{m} \pm 3.7$ ), along with rare polygonal and spindle-shaped interneurons (mean diameter:  $18 \mu\text{m} \pm 5.6$  -  $22 \mu\text{m} \pm 4.5$ ;  $22.3 \mu\text{m} \pm 2$  -  $22.8 \mu\text{m} \pm 2.4$ , respectively). In layers III and IV, polygonal (mean diameter:  $18 \mu\text{m} \pm 2.2$  -  $24.5 \mu\text{m} \pm 3.6$ ;  $17.8 \mu\text{m} \pm 2.7$  -  $25 \mu\text{m} \pm 4.1$ , respectively), with axonal projections, and spheroid interneurons (mean diameter:  $14.8 \mu\text{m} \pm 1.8$  -  $18.9 \mu\text{m} \pm 2$ ;  $14.5 \mu\text{m} \pm 2.5$  -  $17.4 \mu\text{m} \pm 2.6$ , respectively) were present. Spindle-shaped interneurons (mean diameter:  $21.9 \mu\text{m} \pm 3.3$  -  $24 \mu\text{m} \pm 2.8$ ;  $20.4 \mu\text{m} \pm 2.9$  -  $23.1 \mu\text{m} \pm 4.1$ , respectively) were also occasionally observed in these layers. In layers V and VI, polygonal interneurons (mean diameter:  $20.2 \mu\text{m} \pm 3.1$  -  $27.7 \mu\text{m} \pm 3.8$ ;  $21.1 \mu\text{m} \pm 3.8$  -  $26.1 \mu\text{m} \pm 4.5$ , respectively) were present, along with a smaller number of spheroid interneurons (mean diameter:  $15 \mu\text{m} \pm 1.9$  -  $19.2 \mu\text{m} \pm 3$ ;  $16.6 \mu\text{m} \pm 3.5$  -  $20.4 \mu\text{m} \pm 3$ , respectively) and rare spindle-shaped interneurons (mean diameter:  $20.5 \mu\text{m} \pm 3.2$  -  $24.1 \mu\text{m} \pm 3.7$ ;  $23.1 \mu\text{m} \pm 3.2$  -  $25.2 \mu\text{m} \pm 3.3$ , respectively).

## Discussion

In this study, we provided a detailed description of the cytoarchitecture and myeloarchitecture of the sheep auditory cortex, shedding light on its structural organization. PV staining further contributed to understanding its functional properties by highlighting key GABAergic interneurons. These findings deepen our knowledge of the auditory cortex in sheep, an important model for investigating sensory processing in large mammals.

The mean cortical thickness of the sheep auditory cortex ( $1649 \mu\text{m}$ , min:  $1280 \mu\text{m}$ ; max:  $2116 \mu\text{m}$ ) was consistent with the cortical thickness of other regions of the sheep brain reported in previous studies. Among these regions, the primary visual cortex has been reported to be the thinnest ( $1488 \mu\text{m}$ ; [Graïc et al., 2022](#)), followed by the auditory cortex and the orbitofrontal cortex ( $1697 \mu\text{m}$ ; Gerussi et al., 2022). In contrast, the motor cortex exhibits the greatest thickness ( $1838 \mu\text{m}$ ; Peruffo et al.,

2019). Moreover, the six-layer laminar organization observed in the sheep auditory cortex is consistent with findings in the auditory cortices of other mammals (reviewed in, Kaas, 2011). This suggests a somewhat conserved structural organization, and potentially common auditory processing mechanisms, across mammalian species.

Among the six cortical layers, layer II was the thinnest, which is consistent with other regions of the sheep brain (Graïc et al., 2022; Rose, 1942) and in the cortex of other cetartiodactyls (Graïc et al., 2024; Hof et al., 1999). In addition, this layer exhibited the highest cell density, consistent with findings in mammals (Winer, 1985). Layer IV was also relatively thin but its boundaries were more challenging to delineate from adjacent layers. These observations mirror findings in other primary sensory areas, such as the primary visual cortex of sheep (Graïc et al., 2022; Rose, 1942), where layer IV is present but difficult to identify.

Immunostaining for MBP and PV revealed the highest fiber density in layers III to V, which is consistent with studies in other mammals, where these layers are known to harbor dense projections (Hof et al., 1999; Jones et al., 1995; Kaas, 2011; Wallace et al., 1991). The dense MBP-ir myelin and PV-ir fibers suggest a developed network of connections mediated by interneurons, facilitating both local processing, cortico-cortical, and thalamo-cortical communication within the sheep auditory cortex.

Interestingly, we identified basket-like structures exclusively in the upper part of layer V using PV immunostaining. These structures, based on their distinctive morphology and size, likely surround large pyramidal cells. Such large pyramidal cells were observed in the upper part of layer V with cresyl violet staining. This arrangement suggests that the basket-like structures may modulate the activity of pyramidal cells through GABAergic synapsing, potentially playing a pivotal role in regulating excitatory output from layer V, which was previously reported in other mammals (Hof et al., 1999). Additionally, long axonal projections were observed extending into layer II, which may correspond to the projections of large pyramidal neurons. This anatomical configuration suggests a complex interplay between inhibitory and excitatory elements, with basket-like structures potentially contributing to local inhibitory regulation of excitatory pyramidal cells, crucial for auditory information processing.



PV staining has already been used as an indicator of the location of the primary auditory cortex (Kaas & Hackett, 2000). In our study, high density of PV-ir cell bodies was observed in the dorsal part of the posterior ectosylvian gyrus, with staining decreasing ventrally, both into the suprasylvian sulcus and along the outer cortical surface. These observations suggest that the sheep primary auditory cortex is located in the dorsal posterior ectosylvian gyrus, maybe between the internal and intermediate ROIs of the anterior and medial sections, which broadly corresponds to tracing results (Michaloudi et al., 1986). However, further functional studies are needed to confirm the precise location of the primary auditory cortex in sheep.

## **Conclusion**

In this study, we delineated six cortical layers within the sheep auditory cortex in the anterior part of the posterior ectosylvian gyrus, with distinct cell types, distribution, and fiber organization. Additionally, we observed increased parvalbumin staining in the dorsal part of this region, which may correspond to the primary auditory cortex. These findings are consistent with existing literature on the auditory cortex in sheep and other mammalian species. Together, these results suggest that both the structural and functional organization of the auditory cortex are conserved across species, supporting the idea of an evolutionary conservation of auditory processing mechanisms in mammals.

## References

- Anderson, L. A., Christianson, G. B., & Linden, J. F. (2009). Mouse auditory cortex differs from visual and somatosensory cortices in the laminar distribution of cytochrome oxidase and acetylcholinesterase. *Brain Research*, 1252, 130–142.  
<https://doi.org/10.1016/j.brainres.2008.11.037>
- Bagley, C., JR. (1922). Cortical motor mechanism of the sheep brain. *Archives of Neurology & Psychiatry*, 7(4), 417–453. <https://doi.org/10.1001/archneurpsyc.1922.02190100002001>
- Bajo, V. M., Nodal, F. R., Bizley, J. K., Moore, D. R., & King, A. J. (2007). The ferret auditory cortex: Descending projections to the inferior colliculus. *Cerebral Cortex (New York, N.Y.: 1991)*, 17(2), 475–491. <https://doi.org/10.1093/cercor/bhj164>
- Bankhead, P., Loughrey, M. B., Fernández, J. A., Dombrowski, Y., McArt, D. G., Dunne, P. D., McQuaid, S., Gray, R. T., Murray, L. J., Coleman, H. G., James, J. A., Salto-Tellez, M., & Hamilton, P. W. (2017). QuPath: Open source software for digital pathology image analysis. *Scientific Reports*, 7(1), 16878. <https://doi.org/10.1038/s41598-017-17204-5>
- Budinger, E., Heil, P., & Scheich, H. (2000). Functional organization of auditory cortex in the Mongolian gerbil (*Meriones unguiculatus*). III. Anatomical subdivisions and corticocortical connections. *The European Journal of Neuroscience*, 12(7), 2425–2451.  
<https://doi.org/10.1046/j.1460-9568.2000.00142.x>
- Chengetanai, S., Bhagwandin, A., Bertelsen, M. F., Hård, T., Hof, P. R., Spocter, M. A., & Manger, P. R. (2020). The brain of the African wild dog. III. The auditory system. *The Journal of Comparative Neurology*, 528(18), 3229–3244.  
<https://doi.org/10.1002/cne.24989>
- Clarke, P. G., Donaldson, I. M., & Whitteridge, D. (1976). Binocular visual mechanisms in cortical areas I and II of the sheep. *The Journal of Physiology*, 256(3), 509–526.
- Clarke, P. G., & Whitteridge, D. (1976). The cortical visual areas of the sheep. *The Journal of*

- Physiology*, 256(3), 497–508. <https://doi.org/10.1113/jphysiol.1976.sp011335>
- Cook, C. J., Williams, C., & Gluckman, P. D. (1987). Brainstem auditory evoked potentials in the fetal sheep, in utero. *Journal of Developmental Physiology*, 9(5), 429–439.
- Cruikshank, S. J., Killackey, H. P., & Metherate, R. (2001). Parvalbumin and calbindin are differentially distributed within primary and secondary subregions of the mouse auditory forebrain. *Neuroscience*, 105(3), 553–569.  
[https://doi.org/10.1016/s0306-4522\(01\)00226-3](https://doi.org/10.1016/s0306-4522(01)00226-3)
- De Venecia, R. K., Smelser, C. B., & McMullen, N. T. (1998). Parvalbumin is expressed in a reciprocal circuit linking the medial geniculate body and auditory neocortex in the rabbit. *Journal of Comparative Neurology*, 400(3), 349–362.  
[https://doi.org/10.1002/\(SICI\)1096-9861\(19981026\)400:3<349::AID-CNE5>3.0.CO;2-8](https://doi.org/10.1002/(SICI)1096-9861(19981026)400:3<349::AID-CNE5>3.0.CO;2-8)
- Dinopoulos, A., Karamanlidis, A. N., Papadopoulos, G., Antonopoulos, J., & Michaloudi, H. (1985). Thalamic projections to motor, prefrontal, and somatosensory cortex in the sheep studied by means of the horseradish peroxidase retrograde transport method. *The Journal of Comparative Neurology*, 241(1), 63–81.  
<https://doi.org/10.1002/cne.902410106>
- Ebinger, P. (1975). Quantitative investigations of visual brain structures in wild and domestic sheep. *Anatomy and Embryology*, 146(3), 313–323. <https://doi.org/10.1007/BF00302177>
- Gerussi, T., Graić, J.-M., Grandis, A., Peruffo, A., & Cozzi, B. (2022). The orbitofrontal cortex of the sheep. Topography, organization, neurochemistry, digital tensor imaging and comparison with the chimpanzee and human. *Brain Structure and Function*, 227(5), 1871–1891. <https://doi.org/10.1007/s00429-022-02479-w>
- Gierthmuehlen, M., Wang, X., Gkogkidis, A., Henle, C., Fischer, J., Fehrenbacher, T., Kohler, F., Raab, M., Mader, I., Kuehn, C., Foerster, K., Haberstroh, J., Freiman, T. M., Stieglitz, T., Rickert, J., Schuettler, M., & Ball, T. (2014). Mapping of sheep sensory cortex with a novel microelectrocorticography grid. *The Journal of Comparative Neurology*, 522(16),

3590–3608. <https://doi.org/10.1002/cne.23631>

Graïc, J.-M., Corain, L., Finos, L., Vadori, V., Grisan, E., Gerussi, T., Orekhova, K., Centelleghé, C., Cozzi, B., & Peruffo, A. (2024). Age-related changes in the primary auditory cortex of newborn, adults and aging bottlenose dolphins (*Tursiops truncatus*) are located in the upper cortical layers. *Frontiers in Neuroanatomy*, 17.

<https://doi.org/10.3389/fnana.2023.1330384>

Graïc, J.-M., Peruffo, A., Corain, L., Finos, L., Grisan, E., & Cozzi, B. (2022). The primary visual cortex of Cetartiodactyls: Organization, cytoarchitectonics and comparison with perissodactyls and primates. *Brain Structure and Function*, 227(4), 1195–1225.

<https://doi.org/10.1007/s00429-021-02392-8>

Griffiths, S. K., Pierson, L. L., Gerhardt, K. J., Abrams, R. M., & Peters, A. J. M. (1994). Noise induced hearing loss in fetal sheep. *Hearing Research*, 74(1), 221–230.

[https://doi.org/10.1016/0378-5955\(94\)90190-2](https://doi.org/10.1016/0378-5955(94)90190-2)

Hackett, T. A., Preuss, T. M., & Kaas, J. H. (2001). Architectonic identification of the core region in auditory cortex of macaques, chimpanzees, and humans. *The Journal of Comparative Neurology*, 441(3), 197–222. <https://doi.org/10.1002/cne.1407>

Hof, P. R., Glezer, I. I., Condé, F., Flagg, R. A., Rubin, M. B., Nimchinsky, E. A., & Vogt Weisenhorn, D. M. (1999). Cellular distribution of the calcium-binding proteins parvalbumin, calbindin, and calretinin in the neocortex of mammals: Phylogenetic and developmental patterns. *Journal of Chemical Neuroanatomy*, 16(2), 77–116.

[https://doi.org/10.1016/s0891-0618\(98\)00065-9](https://doi.org/10.1016/s0891-0618(98)00065-9)

Jeffrey, M., Wells, G. A., & Bridges, A. W. (1990). An immunohistochemical study of the topography and cellular localization of three neural proteins in the sheep nervous system. *Journal of Comparative Pathology*, 103(1), 23–35.

[https://doi.org/10.1016/s0021-9975\(08\)80132-6](https://doi.org/10.1016/s0021-9975(08)80132-6)

Johnson, J. I., Rubel, E. W., & Hatton, G. I. (1974). Mechanosensory projections to cerebral

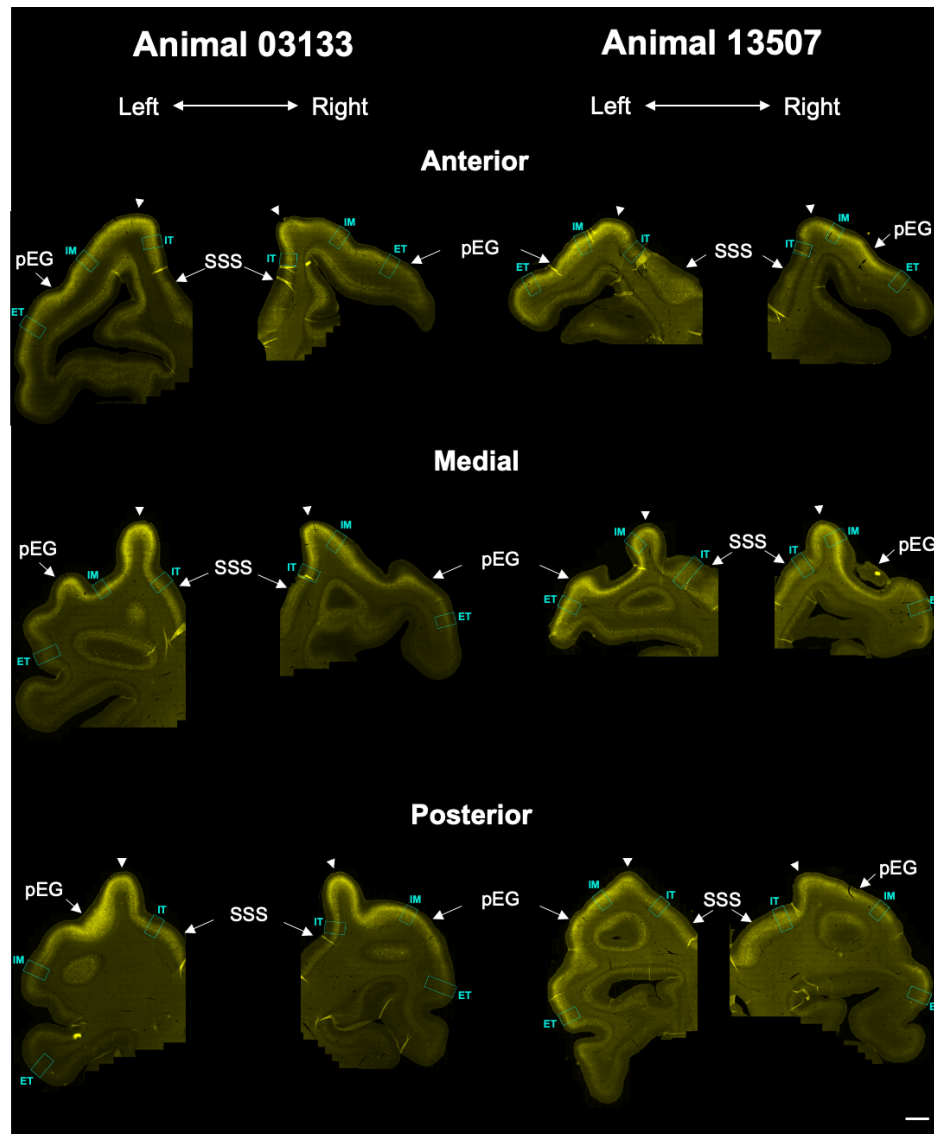
- cortex of sheep. *The Journal of Comparative Neurology*, 158(1), 81–107.  
<https://doi.org/10.1002/cne.901580106>
- Jones, E. G., Dell'Anna, M. E., Molinari, M., Rausell, E., & Hashikawa, T. (1995). Subdivisions of macaque monkey auditory cortex revealed by calcium-binding protein immunoreactivity. *The Journal of Comparative Neurology*, 362(2), 153–170.  
<https://doi.org/10.1002/cne.903620202>
- Kaas, J. H. (2011). The Evolution of Auditory Cortex: The Core Areas. In J. A. Winer & C. E. Schreiner (Eds.), *The Auditory Cortex* (pp. 407–427). Springer US.  
[https://doi.org/10.1007/978-1-4419-0074-6\\_19](https://doi.org/10.1007/978-1-4419-0074-6_19)
- Kaas, J. H., & Hackett, T. A. (2000). The core fields are the most darkly stained. *Proceedings of the National Academy of Sciences*, 97(22), 11793–11799.  
<https://doi.org/10.1073/pnas.97.22.11793>
- Karamanlidis, A. N., Saigal, R. P., Giolli, R. A., Mangana, O., & Michaloudi, H. (1979). Visual thalamocortical connections in sheep studied by means of the retrograde transport of horseradish-peroxidase. *The Journal of Comparative Neurology*, 187(2), 245–260.  
<https://doi.org/10.1002/cne.901870202>
- King, J. L. (1911). Localisation of the motor area in the sheep's brain by the histological method. *Journal of Comparative Neurology*, 21(3), 311–321.  
<https://doi.org/10.1002/cne.900210305>
- Kosaki, H., Hashikawa, T., He, J., & Jones, E. G. (1997). Tonotopic organization of auditory cortical fields delineated by parvalbumin immunoreactivity in macaque monkeys. *The Journal of Comparative Neurology*, 386(2), 304–316.
- Martin del Campo, H., Measor, K., & Razak, K. A. (2014). Parvalbumin and calbindin expression in parallel thalamocortical pathways in a gleaning bat, *Antrozous pallidus*. *The Journal of Comparative Neurology*, 522(10), 2431–2445. <https://doi.org/10.1002/cne.23541>
- McMullen, N. T., Smelser, C. B., & de Venecia, R. K. (1994). A quantitative analysis of

- parvalbumin neurons in rabbit auditory neocortex. *The Journal of Comparative Neurology*, 349(4), 493–511. <https://doi.org/10.1002/cne.903490402>
- Michaloudi, H., Karamanlidis, A. N., Dinopoulos, A., Papadopoulos, G., & Antonopoulos, J. (1986). Thalamic projections to the posterior sylvian and posterior ectosylvian gyri of the sheep brain, revealed with the retrograde transport of horseradish peroxidase. *Anatomy and Embryology*, 175(1), 77–90. <https://doi.org/10.1007/BF00315458>
- Peruffo, A., Corain, L., Bombardi, C., Centelleghes, C., Grisan, E., Graïc, J.-M., Bontempi, P., Grandis, A., & Cozzi, B. (2019). The motor cortex of the sheep: Laminar organization, projections and diffusion tensor imaging of the intracranial pyramidal and extrapyramidal tracts. *Brain Structure & Function*, 224(5), 1933–1946. <https://doi.org/10.1007/s00429-019-01885-x>
- Pierson, L. L., Gerhardt, K. J., Abrams, R. M., Griffiths, S. K., & Peters, A. J. (1994). Effect of impulse noise on the auditory brainstem response of the fetal sheep and the adult ewe: Case study. *Military Medicine*, 159(11), 676–680.
- Pierson, L. L., Gerhardt, K. J., Griffiths, S. K., & Abrams, R. M. (1995). Auditory brainstem response in sheep. Part I: Fetal development. *Developmental Psychobiology*, 28(5), 293–305. <https://doi.org/10.1002/dev.420280505>
- Roberto, M., Hamernik, R. P., & Turrentine, G. A. (1989). Damage of the auditory system associated with acute blast trauma. *The Annals of Otology, Rhinology & Laryngology. Supplement*, 140, 23–34. <https://doi.org/10.1177/00034894890980s506>
- Rose, J. E. (1942). A cytoarchitectural study of the sheep cortex. *Journal of Comparative Neurology*, 76(1), 1–55. <https://doi.org/10.1002/cne.900760102>
- Sahasrabudde, K., Khan, A. A., Singh, A. P., Stern, T. M., Ng, Y., Tadi, A., Orel, P., LaReau, C., Pouzner, D., Nishimura, K., Boergens, K. M., Shivakumar, S., Hopper, M. S., Kerr, B., Hanna, M.-E. S., Edgington, R. J., McNamara, I., Fell, D., Gao, P., ... Angle, M. R. (2021). The Argo: A high channel count recording system for neural recording in vivo. *J.*

*Neural Eng.*

- Simpson, S., & King, J. L. (1911). Localisation of the Motor Area in the Sheep. *Quarterly Journal of Experimental Physiology*, 4(1), 53–65.  
<https://doi.org/10.1113/expphysiol.1911.sp000083>
- Wallace, M. N., Kitzes, L. M., & Jones, E. G. (1991). Chemoarchitectonic organization of the cat primary auditory cortex. *Experimental Brain Research*, 86(3), 518–526.  
<https://doi.org/10.1007/BF00230525>
- Winer, J. A. (1985). Structure of layer II in cat primary auditory cortex (AI). *The Journal of Comparative Neurology*, 238(1), 10–37. <https://doi.org/10.1002/cne.902380103>
- Winer, J. A., & Prieto, J. J. (2001). Layer V in cat primary auditory cortex (AI): Cellular architecture and identification of projection neurons. *The Journal of Comparative Neurology*, 434(4), 379–412. <https://doi.org/10.1002/cne.1183>
- Woolsey, C. N., & Fairman, D. (1946). Contralateral, ipsilateral, and bilateral representation of cutaneous receptors in somatic areas I and II of the cerebral cortex of pig, sheep, and other mammals. *Surgery*, 19, 684–702.

## Supplementary material



**Supplementary Figure 1. Dorsoventral gradient of PV staining in the sheep auditory cortex.** The three sections (anterior, medial, posterior) are represented for both hemispheres of animals 03133 and 13507. The three ROIs (IT, IM, ET) are indicated in blue for each section. A dorsoventral gradient in PV staining density is observed, with the highest density in the dorsal part of the posterior ectosylvian gyrus (white arrowhead). The gradient decreases abruptly into the suprasylvian sulcus (SSS) and more gradually along the outer cortical surface (pEG). Scale bar at bottom right applied for all sections: 2000  $\mu\text{m}$ .